

# Forward Roll Coating Flows of Viscoelastic Liquids

G. A. Zavallos<sup>1,2</sup>, M. S. Carvalho<sup>1</sup>, M. Pasquali<sup>2</sup>

<sup>1</sup>*Department of Mechanical Engineering, Pontificia Universidade Catolica do Rio de Janeiro, Rua Marques de Sao Vicente 225, Gavea, Rio de Janeiro, RJ, 22453-900, Brazil*

<sup>2</sup>*Department of Chemical Engineering – MS 362, Rice University, 6100 Main St, Houston, TX, 77005, USA*

## Abstract

Except at low speed, the film splitting flow that occurs in forward roll coating is three-dimensional and results in more or less regular stripes in the machine direction. For Newtonian liquids, the stability of the film-split flow is determined by the competition of capillary forces and viscous forces: the onset of meniscus nonuniformity is marked by a critical value of the capillary number. Although most of the liquids coated industrially are polymeric solutions and dispersions that are not Newtonian, most of previous theoretical analyses of film splitting flows dealt only with Newtonian liquids. Non-Newtonian behavior can drastically change the nature of the flow near the free surface; when minute amounts of flexible polymer are present, the onset of the three-dimensional instability occurs at much lower speeds than in the Newtonian case.

This free surface coating flow is analyzed here with differential constitutive models, the Oldroyd-B and the FENE-P equations. The continuity and momentum equations coupled with the constitutive models, and the non-linear mapping equations that transform the free boundary problem into a fixed boundary problem are solved with the DEVSS-G/SUPG method with finite element basis functions. The resulting set of non linear equations is solved by Newton's method with pseudo-arc-length continuation. The results show how the flow field changes with Weissenberg number, leading to changes in the forces at a free surface that may explain why the the ribbing instability sets in at smaller Capillary number when the liquid is viscoelastic.

## 1 Introduction

Roll coating is widely used to apply a thin liquid layer to a continuous, flexible substrate. Except at low speeds, the flow is three-dimensional and results in more or less regular stripes in the machine direction. This type of instability, or rather the three-dimensional flow to which it may lead, is commonly called *ribbing*. It limits the speed of the process if a smooth film is required as a final product.

The flow and the instability of the splitting of a Newtonian liquid as it exits from between two rotating rolls has been extensively studied. Pearson [1] first explained why a flow that otherwise leads to a uniform meniscus can turn unstable. He showed that the adverse pressure gradient near the film-split meniscus necessary to decelerate the flowing liquid destabilizes the free surface, whereas surface tension stabilizes it. A critical value of the ratio between these two forces, i.e. the capillary number  $Ca \equiv \mu V / \sigma$ , marks the onset of the free surface nonuniformity. Here,  $\mu$  is the liquid viscosity,  $\sigma$  its surface tension and  $V$  is the mean roll speed.

Several experimental and theoretical studies of the film-splitting instability of Newtonian liquids between rigid rolls have been published [2, 3, 4, 5, 6, 7].

In practice, coating solutions often contain polymers. Non-Newtonian behavior can drastically change the nature of the flow near the free surface and consequently alter the performance of a coater. Most of the analyses of viscoelasticity in roll coating consisted of experimentally testing the effect of certain polymer additives on the ribbing stability [8, 9, 10, 11, 12, 13, 14]. Limited theoretical analyses of stability of viscoelastic film splitting flows have appeared [15]; recently, a mechanism has been proposed that shows that the hoop stresses at a stretching free surface caused by a locally extensional flow would destabilize the surface with respect to spanwise perturbations [16]. Coupled with the computational analysis of Refs. [17, 18], which show that the maximum polymer extension is always attained *downstream* of a stagnation point on a free surface, the analysis of Ref. [16] has an interesting implication for film-splitting flows: if a recirculation is present at the film split, then the instability should start downstream of the second stagnation point on the free surface after the film split location; conversely, if a recirculation is absent, the instability should start near the film split location.

Accurate theoretical predictions of the onset of ribbing when viscoelastic liquids are used is still not available. The mechanisms by which the liquid elasticity makes the flow unstable at Capillary numbers much lower than in the Newtonian case is poorly understood. In order to model any flow instability, it is crucial to develop accurate theoretical analysis of both the base flow, in this case steady and two-dimensional, and the response of that flow to all physically admissible infinitesimal disturbances.

Coating flow modeling must rely on theories that can account for the different behavior of microstructured liquids in shear and extensional flow. Moreover, coating flows always involve free surfaces and contact lines. The domain where the differential equations are posed is unknown *a priori* and it is part of the solution. These two characteristics make the problem extremely complex and they are the main reason why complete two dimensional solutions of viscoelastic free surface

flows are rare [17, 18, 19].

In this work, the two-dimensional, viscoelastic free surface flow near the film split meniscus of a forward roll coating gap is analyzed by solving with the Finite Element method the momentum and continuity equations coupled with the Oldroyd-B and FENE-P differential constitutive models. The results show how the liquid properties affect the stress field near the film split free surface and reveal an elastic mechanism that may explain the early onset of the three-dimensional instability when viscoelastic liquids are used.

## 2 Mathematical Model

### 2.1 Governing Equations

For incompressible, isothermal flow, the momentum and continuity equations are:

$$\rho \mathbf{v} \cdot \nabla \mathbf{v} - \nabla \cdot \mathbf{T} = \mathbf{0} \quad \text{and} \quad \nabla \cdot \mathbf{v} = 0. \quad (1)$$

where  $\rho$  is the liquid density and  $\mathbf{T} \equiv -p\mathbf{I} + \boldsymbol{\tau} + \boldsymbol{\sigma}$  is the total stress tensor, the sum of pressure  $p$ , viscous  $\boldsymbol{\tau}$  and elastic stress  $\boldsymbol{\sigma}$ . The viscous stress obeys Newton's law of viscosity,

$$\boldsymbol{\tau} = 2\mu\mathbf{D}. \quad (2)$$

$\mu$  is the solvent viscosity and  $\mathbf{D}$  is the rate of strain tensor.

The salient microstructural features of a flowing polymer solution are the stretch and orientation of the polymer chains (conformation), and their degree of entanglement. The model used here is restricted to non-entangled liquids. The conformation of the flowing liquid is represented by the conformation dyadic  $\mathbf{M}$ , and its behavior is specified through constitutive assumptions on the functions that appear in its transport equation [20, 17]. Regarding molecular stretch, orientation, and relaxation as independent, taking the vorticity as the average rate of rotation of the polymer molecules, and using isotropy and representation theorems, the equation of change of conformation can be written as [17]

$$\begin{aligned} \frac{\partial \mathbf{M}}{\partial t} + \mathbf{v} \cdot \nabla \mathbf{M} - 2\xi \frac{\mathbf{D} : \mathbf{M}}{\mathbf{I} : \mathbf{M}} \mathbf{M} - \zeta (\mathbf{M} \cdot \mathbf{D} + \mathbf{D} \cdot \mathbf{M} - 2 \frac{\mathbf{D} : \mathbf{M}}{\mathbf{I} : \mathbf{M}} \mathbf{M}) \\ - \mathbf{M} \cdot \mathbf{W} - \mathbf{W}^T \cdot \mathbf{M} + \frac{1}{\lambda} (g_0 \mathbf{I} + g_1 \mathbf{M} + g_2 \mathbf{M}^2) = 0 \end{aligned} \quad (3)$$

where  $\mathbf{W}$  is the vorticity tensor,  $\lambda$  is the characteristic relaxation time of the polymer,  $\xi(\mathbf{M})$  and  $\zeta(\mathbf{M})$  represent the resistance to stretching and relative rotation of polymer segments, and  $g_0(\mathbf{M})$ ,  $g_1(\mathbf{M})$  and  $g_2(\mathbf{M})$  define the rate of relaxation of the polymer segments. The different constitutive models can be obtained by specifying the appropriate form of the constitutive functions  $\xi$ ,  $\zeta$ ,  $g_0$ ,  $g_1$  and  $g_2$ . Summary tables of these forms are in Refs. [20, 21, 17].

The relationship between elastic stress and conformation can be obtained from the local rate of entropy production and the Clausius-Duhem inequality:

$$\boldsymbol{\sigma} = 2\rho(\xi - \zeta) \frac{\mathbf{M}}{\mathbf{I} : \mathbf{M}} \mathbf{M} : \frac{\partial a}{\partial \mathbf{M}} + 2\rho\zeta \mathbf{M} \cdot \frac{\partial a}{\partial \mathbf{M}} \quad (4)$$

where  $a(T, \mathbf{M})$  is the specific free energy of the viscoelastic liquid.

Two different constitutive models—Oldroyd-B and FENE-P—were used in this work. In both models, the molecules follow imposed large-scale deformation affinely. In the Oldroyd-B model, the rate of relaxation of the molecules is a linear function of how far the conformation tensor  $\mathbf{M}$  is away from its equilibrium value  $\mathbf{I}$ . In the FENE-P model, the maximum extension of the molecules is finite, and their rate of relaxation grows infinitely fast as the average molecular extension approaches its maximum value. The form of the constitutive functions and the free energy for each model are:

Constitutive Model	$\xi$	$\zeta$	$g_0$	$g_1$	$g_2$	$a(\mathbf{M})$
Oldroyd-B	1	1	-1	1	0	$G/(2\rho \text{tr} \mathbf{M})$
FENE-P	1	1	-1	$\frac{b-1}{b-\text{tr} \mathbf{M}/3}$	0	$\frac{3}{2}G(b-1) \ln \left[ \frac{b-1}{b-\text{tr} \mathbf{M}/3} \right]$

The relationship between the elastic stress and the conformation tensor, eq.(4), is rewritten in order to enforce  $p = -(1/3)\text{tr}(\mathbf{T})$ . The rheological parameters are the polymer elastic modulus  $G$ , the relaxation time  $\lambda$ , and the ratio of the maximum length square of the polymer molecules to their average length square at equilibrium  $b$  (only for FENE-P). In all the models, the polymer viscosity  $\eta_p$  can be defined as a function of the elastic modulus and relaxation time,  $\eta_p = G\lambda$ .

The boundary conditions are flooded condition and fully developed elastic stress at the inlet; no slip and no penetration at the roll surfaces; force balance and kinematic condition at the free surface; and fully developed flow at the outlet.

## 2.2 Solution Method

Because of the free surfaces, the flow domain at each parameter is unknown *a priori*. In order to solve this free boundary problem by means of standard techniques for boundary value problems, the set of differential equations and boundary conditions posed in the unknown domain  $\Omega$  has to be transformed to an equivalent set defined in a known reference domain  $\Omega_0$ . Detailed description of methods to solve free boundary problems are presented in Refs. [22, 23, 24].

The set of differential equations that describe the conservation of momentum and mass (1), the evolution of the polymer conformation (3), and define the mapping between the physical and reference domain, together with the algebraic equations for the viscous and elastic stresses are all solved on the reference domain  $\Omega_0$  by the Finite Element Method [17, 18, for details].

Computational methods to solve viscoelastic flows are still an active area of research, and several methods of solving the partial differential equations of such flows have been proposed in recent years [25, for a recent review]. The method

used here is the modification of the DEVSS-G/SUPG finite element method [26, 27] developed by Pasquali [17, 18]. As in DEVSS-G, an additional variable  $\mathbf{L}$  (called the interpolated velocity gradient) is introduced to have a continuous representation of the velocity gradient field; unlike in DEVSS-G, it is defined to be traceless by construction [17, 18]

$$\mathbf{L} - \nabla \mathbf{v} + \frac{1}{\text{tr} \mathbf{I}} (\nabla \cdot \mathbf{v}) \mathbf{I} = \mathbf{0} \quad (5)$$

Each variable is approximated with a finite combination of basis functions: Lagrangian biquadratic for position and velocity, linear discontinuous for pressure, and Lagrangian bilinear for interpolated velocity gradient and conformation. Galerkin weighting is used for mesh generation, momentum, continuity, and velocity gradient interpolation. The conformation transport equation is weighted with the Streamline-Upwind Petrov-Galerkin method,  $\psi_{\mathbf{M}} \equiv \phi_{\mathbf{M}} + h^u \mathbf{v} \cdot \nabla \phi_{\mathbf{M}}$ . The upwind parameter  $h^u$  coincides with the characteristic size of the smallest element in the finite element mesh.

The set of nonlinear algebraic equations that arises from applying the method of weighted residuals and the variables representation in terms of basis functions is solved by Newton's method with analytical Jacobian and first order arclength continuation. Three different meshes are used. The main difference between them is the level of refinement near the free surface. Mesh 1 has 20 element across the film thickness, 60 elements along the film split free surface and 49,260 total degrees of freedom. Mesh 2 has 30 elements across the film thickness and 90 elements along the free surface, and 109,525 degrees of freedom. The finest mesh, Mesh 3, has 40 elements across the film thickness, 120 elements along the free surface and 193,548 degrees of freedom.

### 3 Results

The important dimensionless parameters for the flow studied here are: Reynolds number  $Re = \rho VR/H_0$ , Capillary number  $Ca = \mu V/\sigma$ , dimensionless gap  $H_0/R$ , Weissenberg number  $We = \lambda V/H_0$ , solvent to total viscosity ratio  $\beta = \mu/(\mu + \eta_p)$ , polymer extensibility (when using FENE-P model)  $b$ . The predictions presented here are for vanishing Reynolds number and fixed dimensionless gap  $H_0/R = 0.01$ .

#### 3.1 Newtonian Liquids

The film splitting flow is strongly affected by capillary number. When surface tension is strong compared to viscous forces (low capillary number), the meniscus is pulled away from the gap and a large recirculation attached to the free surface is formed. As the capillary number rises, the meniscus recedes and the recirculation disappears, as shown in Fig. 1. Because the rolls are rotating at equal speed, the flow is symmetric and only half of the domain is shown. At  $Ca = 2$  there is only one stagnation point at the free surface, located at the mid-plane between the rolls.

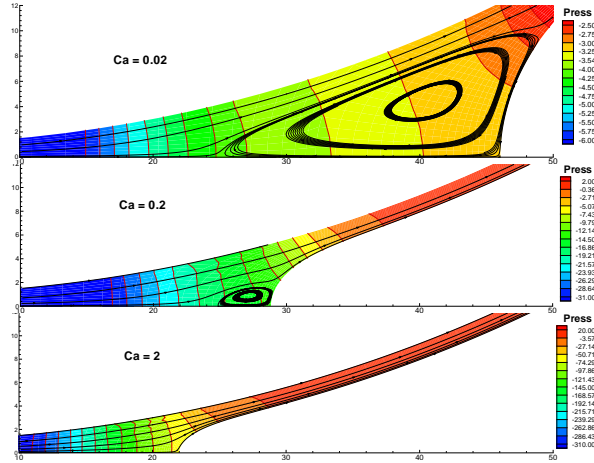


Figure 1: Streamlines and pressure vs. capillary number, Newtonian flow.

The predicted flow rate in units of roll speed times gap, and consequently the film thickness, is virtually constant with capillary number, and approximately equal to  $q \equiv Q/(2VH_0) = 1.34$ . The results obtained here reproduce those of Ref. [7].

### 3.2 Viscoelastic Liquids: Oldroyd-B and FENE-P

The flow of a viscoelastic liquid near the film split meniscus of a forward roll coater was modeled with the Oldroyd-B and FENE-P equations. All the predictions shown here were computed at  $\beta = 0.59$ .

Fig. 2 shows the streamlines and the evolution of the normal stress  $T_{xx}$  of the total stress field as a function of the Weissenberg number at  $Ca = 0.2$  obtained with the FENE-P model ( $b = 50$ ). At low  $We$ , the behavior is similar to the Newtonian case, as expected. As the elasticity of the liquid becomes stronger, the region of high normal stress  $T_{xx}$  close to the roll surfaces is shifted downstream, the stress at the intersection between the free surface and the symmetry line falls, and the positive normal stress gradient at the free surface falls, as illustrated in Fig.3(a). The change in the normal stress gradient at the free surface has an important effect on the stability of the flow with respect to three-dimensional perturbations. At even higher Weissenberg number, the normal stress gradient could change sign and become negative, leading to flow instability.

Another important effect of the liquid elasticity is that downstream of the stagnation line at the free surface, where the molecule extension is strong (Fig. 4, the stress rises with Weissenberg number. The normal component  $T_{xx}$  of the stress field along the free surface is shown in Fig. 3(b) at different Weissenberg numbers. As the liquid becomes more viscoelastic, a stress peak is formed downstream of the

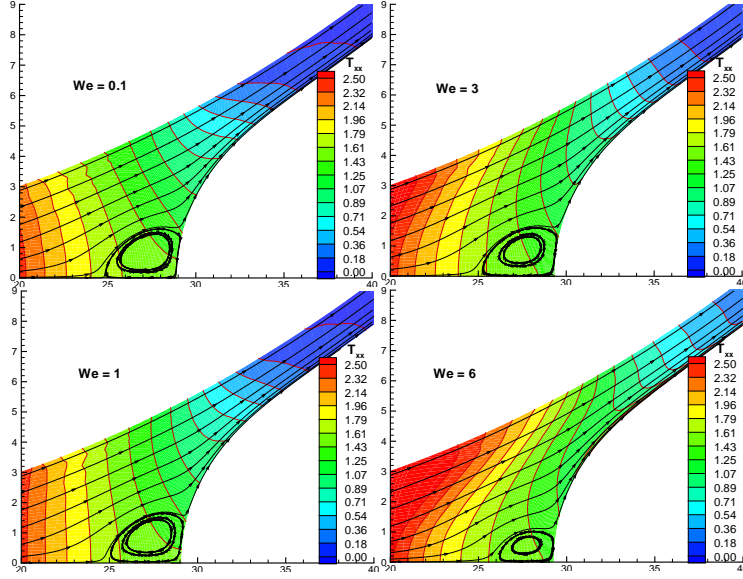


Figure 2: Evolution of the stress component  $T_{xx}$  as a function of Weissenberg number predicted by the FENE-P model.  $b = 50$  and  $Ca = 0.2$ .

stagnation point. The change of the stress gradient along the free surface alters the flow configuration. The positive gradient of the normal stress along the free surface pulls the liquid downstream and reduces the size of the recirculation zone. At  $We = 6$ , the recirculation attached to the film split meniscus has shrunk considerably. As the size of the recirculation diminishes, the velocity gradient at the film split meniscus grows, which induces steeper stress gradients there. At even higher Weissenberg number, the recirculation may disappear completely leading to very high stress gradient at the film split meniscus in the main flow direction which would destabilize the flow with respect to three-dimensional disturbances. This hypothesis could not be confirmed yet, because the flow simulations, with the mesh refinement presented here, were limited to  $We \approx 6$ .

The appearance of elastic stress boundary layers near the liquid/gas interface has been reported in other free surface flows [17, 18, 19]. The liquid elasticity also creates compressive elastic forces in the spanwise direction. At low Weissenberg number, the spanwise stress component is negligible, as expected. As the Weissenberg number rises, the spanwise transverse elastic stress grows negative (compressive stress) because the polymer molecules are extended along the free surface in the streamwise direction and contracted in the two perpendicular directions. Near the film-split free surface, a boundary layer is formed of high compressive stress. Such stress, which is not present in Newtonian liquids, may destabilize the flow with respect to transverse disturbance causing the free surface to buckle.

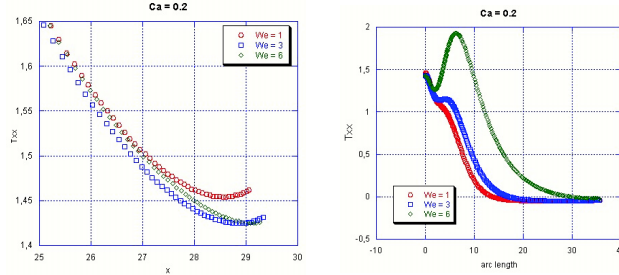


Figure 3: Normal stress component  $T_{xx}$  along the symmetry line (a) and along the free surface (b), at different Weissenberg number.  $Ca = 0.2$ .

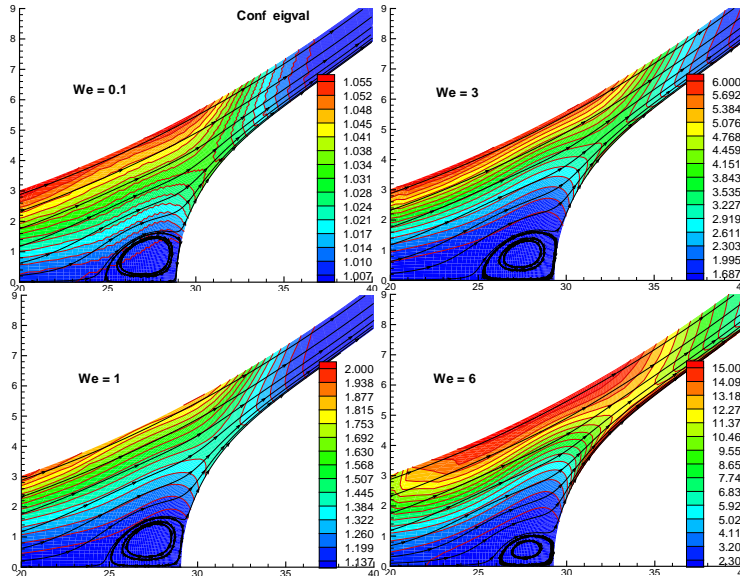


Figure 4: Maximum eigenvalue of conformation tensor as a function of Weissenberg number.

## 4 Final Remarks

In forward roll coating, above a critical capillary number, the two-dimensional film splitting meniscus becomes three-dimensional, resulting in more or less regular stripes in the coated liquid film. For Newtonian liquids, the stability of the two-dimensional flow is determined by a competition of surface tension and viscous forces. Experiments have shown that liquid viscoelasticity destabilizes the flow; when minute amounts of flexible polymer are present, the three-dimensional instability sets in at much lower speeds than in the Newtonian case. The mechanisms

responsible for this early onset of the instability are still under investigation.

The two-dimensional flow of viscoelastic liquids in a forward roll coating gap was analyzed by solving the continuity and momentum equations coupled with two differential constitutive equations, the Oldroyd-B and FENE-P models. The resulting set of differential equations was solved by Galerkin's method and finite element basis functions. The results show that the elastic forces change the flow characteristics near the free surface. At a fixed capillary number, the stresses at the free surface rise because of the strong extensional character of the flow in that region; the normal stress gradient in the main flow direction falls and compressive normal stresses on the transverse direction appear. All these effects destabilize the flow with respect to three-dimensional perturbation and contribute to explaining the early onset of ribbing when viscoelastic liquids are used.

## 5 Acknowledgements

This work was funded by CNPq (Brazilian Research Council, Grant 300242/98-0), by FAPERJ (Research Foundation of the State of Rio de Janeiro, Grant E-26/150.355/2002) by the National Science Foundation (CTS-CAREER-0134389), and by a gift from ExxonMobil. A color version of the article is at <http://www.ruf.rice.edu/~mp/articles/wit2003-VEfilmsplit.pdf>.

## References

- [1] Pearson, J.R.A., The stability of uniform viscous flow under rollers and spreaders. *J. Fluid Mech.*, **7**, 481, 1960.
- [2] Pitts, E. & Greiller, J., The flow of thin liquid films between rollers, *J. Fluid Mech.*, **11**, 33, 1960.
- [3] Mill, C.C. & South, G.R., Formation of ribs on rotating rollers. *J. Fluid Mech.*, **28**, 523, 1967.
- [4] Greener, J., Sullivan, T., Turner, B. & Middleman, S., Ribbing instability of a two-roller coater: Newtonian fluids, *Chem. Eng. Commun.*, **5**, 73, 1980.
- [5] Savage, M., Mathematical Model for the Onset of Ribbing. *AIChE J.*, **30**, 999, 1984.
- [6] Benkreira, H., Edwards, M.F. & Wilkinson, W.L., Ribbing instability in the roll coating of Newtonian fluids. *Plastic and Rubber Proc. Appl.*, **2**, 137, 1982.
- [7] Coyle, D.J., Macosko, C.W. & Scriven, L.E., Stability of symmetric film-splitting between counter-rotating cylinders. *J. Fluid Mech.*, **216**, 437, 1990.
- [8] Bauman, T., Sullivan, T. & Middleman, S., Ribbing instability in coating flows: effect of polymer additives. *Chem. Eng. Commun.*, **14**, 35, 1982.
- [9] Glass, J.E., Dynamics of roll spatter and tracking 1: Commercial latex trade paints. *J. Coating Technol.*, **50**, 53, 1978.
- [10] Fernando, R.H., & Glass, J.E., Dynamic uniaxial extensional viscosity (DUEV) effects in roll applications II: Polymer blend studies. *J. Rheol.*, **32**, 199, 1988.

- [11] Carvalho, M. S., Dontula, P. & Scriven, L. E., Non-Newtonian effects on the Ribbing instabilities. *TAPPI Coating Conference*, Dallas, USA, 1995.
- [12] Grillet, A.M., Lee, A.G. & Shaqfeh, E. S. G., Observations of ribbing instabilities in elastic fluid flows with gravity stabilization. *J. Fluid Mech.*, **399**, 49, 1999.
- [13] Dontula, P., Polymer Solutions in Coating flows. *PhD thesis University of Minnesota, Minneapolis, MN*, 1999.
- [14] Varela-Lopez, F., Pauchard, L., Rosen, M. & Rabaud, M., Non-Newtonian effects on ribbing instability threshold. *J. Non-Newtonian Fluid Mech.*, **103**, 123, 2002.
- [15] Ro, J. S. & Homsy G. M., Viscoelastic free-surface flows thin-film hydrodynamics of Hele-Shaw and dip coating flows. *J. Non-Newtonian Fluid Mech.*, **57**, 203, 1995.
- [16] Graham, M. D., Interfacial hoop stress and instability of viscoelastic free surface flows. *Phys. Fluids*, **15**, 1702, 2003.
- [17] Pasquali, M., Polymer Molecules in Free Surface Coating flows. *PhD thesis University of Minnesota, Minneapolis, MN*, 2000.
- [18] Pasquali, M. & Scriven, L. E., Free surface flows of polymer solutions with models based on the conformation tensor. *J. Non-Newtonian Fluid Mech.*, **108**, 363, 2002.
- [19] Lee, A. G., Shaqfeh, E. & Khomami, B. A study of viscoelastic free surface flows by the finite element method: Hele-Shaw and slot coating flows. *J. Non-Newtonian Fluid Mech.*, **108**, 327, 2002.
- [20] Beris, A. N. & Edwards, B. J., Thermodynamics of flowing systems with internal microstructure. *Oxford University Press*, Oxford, 1994.
- [21] Kwon, Y. & Leonov, A. I., Stability constraints in the formulation of viscoelastic constitutive equations. *J. Non-Newtonian Fluid Mech.*, **58**, 25, 1995.
- [22] Kistler, S. F. & Scriven, L. E., Coating Flows. In “Computational Analysis of polymer processing”, Eds. J. R. A. Pearson and S. M. Richardson. *Applied Science Publisher*, London & New York, 243, 1983.
- [23] Christodoulou, C. N. & Scriven, L. E., Finding leading modes of a viscous free surface flow: An asymmetric generalized eigenproblem. *J. Sci. Comp.*, **3**, 355, 1990.
- [24] Carvalho, M. S. & Scriven, L. E., Three-dimensional stability analysis of free surface flows: Application to forward deformable roll coating. *J. Comput. Phys.*, **151**, 534, 1999.
- [25] Baaijens, F. P. T., Mixed finite element methods for viscoelastic analysis: a review. *J. Non-Newtonian Fluid Mech.*, **79**, 361, 1998.
- [26] Guénette, R. and Fortin, M., A New Finite Element Method for Computing Viscoelastic Flows. *J. Non-Newtonian Fluid Mech.*, **60**, 27, 1995.
- [27] Szady, M. J., Salomon, T. R., Liu, A. W., Armstrong, R. C. & Brown, R. A., A new mixed finite element method for viscoelastic flows governed by differential constitutive equations. *J. Non-Newtonian Fluid Mech.*, **59**, 215, 1995.